A NOVEL CONTROL ARCHITECTURE FOR ROBOTIC-ASSISTED SINGLE INCISION LAPAROSCOPIC SURGERY

DOINA PISLA[1], DONATO CARAMIA[2], BOGDAN GHERMAN[1*], GIOVANNI SOLETI[2], IONUT ULINICI[1], CALIN VAIDA[1]

Abstract. Single Incision Laparoscopic Surgery is a developing procedure which has the potential to become the future of laparoscopic surgery. Its main advantage over the classic laparoscopic surgical interventions consists in its potential of hiding any trace of a surgery operation if achieved through the umbilicus. Nevertheless, this procedure requires highly developed technical equipment in a very narrow space, with large dexterity, for this reason robotics may provide a viable solution. The paper focuses on the development of a robotic SILS instruments architecture and a communication protocol within a master-slave teleoperated robotic system by implementing the client-server approach to transfer information between different devices to render a smooth operation of the equipment, adapted to the medical specialists' needs. The master component is the well-known Omega.7 haptic device, while the slave component consists of the KUKA iiwa LBR collaborative robot which positions the set of custom designed robotic SILS instruments. The inverse kinematics of the instruments has been also developed, to be further used within the control system. A set of simulations using the CoppeliaSim and Matlab environments have been done to show that the proposed solution can potentially be implemented into a fully developed solution.

Key words: robotic surgery, client-server architecture, teleoperation, kinematics, simulation.

1. INTRODUCTION

Minimally invasive laparoscopic surgery (MIS) is considered as a less invasive alternative to open surgery. MIS involves the use of slim surgical instruments and a laparoscope, more recently laparoscopic camera. The instruments and the camera are introduced through trocars placed in multiple incisions into the abdomen [1]. A further evolution of MIS has come under the

[1] Technical University of Cluj-Napoca, 400114 Cluj-Napoca, Romania
[2*] Corresponding author, Politecnico di Bari, 70126 Bari, Italy

form of single incision laparoscopic surgery (SILS). Unlike MIS, SILS is a minimally invasive technique that implies the insertion of the surgical instruments and the laparoscopic camera inside the patient's body, through a single 25 mm incision [1]. The most frequently utilized site for the incision is at the level of the umbilicus, as it has been proven to reduce post-operative scarring of the site. In the case of SILS, the instruments are introduced through trocars as in MIS, with a difference being the use of a device known as a SILS port.

Various types of ports have been developed since the introduction of SILS in surgery [2]. These SILS ports are generally fabricated out of a flexible silicon-like material and are placed within the incision. SILS ports can either have one single entryway (towards the operating site) through which the trocars and ultimately instruments, are introduced, there are also SILS ports that have separate entries for the trocars, aside from these features there are also ports outfitted with a valve that can be used to eliminate gases from the intra-abdominal cavity, which are caused as a biproduct of the surgical procedure. SILS ports are also responsible for maintaining the operation site sealed from the outside as not to allow gaseous exchange between the two environments (interior of the human body and the operating room). The soft constitution of the ports in comparison to conventional trocars could potentially be less damaging to the incision site.

In terms of feasibility SILS has proven itself as a highly efficient technique, providing several advantages over open surgery and MIS. In the last decade, the introduction, use and success of robotics in surgery has led to the development of robotic surgical systems specifically designed for SILS procedures or capable of achieving MIS and SILS [3–10]. Some robotic systems have been evaluated to determine the performance that can be achieved during SILS procedures and have been compared to robotic MIS or conventional Laparoscopic surgery [11–15]. The results of these studies have been mostly similar, in that the mean operative time for robotic assisted SILS (RSILS) is slightly longer than for manual laparoscopy, the learning curve for robotic procedures is smoother, mean post-operative hospitalization is shorter by at most a day for RSILS, post-operative pains have been less frequent for RSILS compared to SILS or MIS and post-operative cosmesis is better in the case of SILS. Other major differences between robotic and manual laparoscopy have been noted to be the result of pre-existing patient conditions, not due to the robotic procedures themselves.

Given the complexity of the surgical procedures, the development of control systems that fit the dynamic of the surgical tasks [16] is imperative in ensuring the dependability of a system and its safety-oriented behavior [17]. Often due to the high importance that is attributed to surgical procedures, well defined protocols must be present as to enable the safe operation of a robotic device even by someone other than the main surgeon. A robot control system can be divided into several stages [18]. There is the User Level, which ensures the interaction of the user with the robot, this is usually done through a graphical user interface (GUI) such as a computer and its peripherals (keyboard, mouse, touch screens, joysticks, microphone, AR/VR devices, etc.). Then there is the command-and-control stage, which generally includes Programmable Logic Controllers (PLC), in this case the PLC generates the electrical signals that are required to actuate the motors, these are dependent on the input data from the user implemented control algorithms. At the physical stage there is the robotic device, the surgical instruments it is using, sensors, etc. In this paper a novel system for RSILS procedures is proposed, comprised of a novel actuated surgical instrument and a KUKA medical robot. The system's functionality is studied in a virtual environment with the purpose of determining the feasibility of a solution implicating the use of already commercially available robotic arms in collaboration with dedicated actuated instruments.

The paper is structured as follows:

- Section 2 presents the design of an innovative robotic SILS instrument and its kinematic analysis,
- Section 3 illustrates the communication architecture between the master (haptic control device) and slave robotic system (Kuka iiwa),
- Section 4 shows several simulation results obtained using the virtual environment, presenting the orientation, and positioning capacity of the system relative to a virtual human model,
- Section 5 contains several conclusions regarding the developed work.

2. THE ROBOTIC SYSTEM FOR SILS

The robotic-assisted SILS system assumes that the surgeon uses a custom designed user interface - the master console - to provide input into (to control) a slave robotic system Fig. 1, [19]. The slave will copy the master's motions in a pre-designed way, ensuring all the safety protocols required by the specific SILS procedure, which may change during the intervention: scale-up or scale-down the master's motions, couple and decouple the slave from the master at the master's decision, etc. Within the proposed configuration, the master console is the Omega.7 by Force Dimension [20], a 7 Degrees of Freedom (DoF) haptic device having a hybrid structure comprised of a parallel Delta architecture in series with a Roll-Pitch-Yaw wrist and a finger gripper. The slave system consists of the KUKA iiwa LBR 7 R800 collaborative robot which is used to position and orient a mounting platform holding custom designed SILS robotic instruments, namely two identical robotic instruments (the Right and Left hand of the surgeon, each one controlled by a dedicated Omega.7 device) and a laparoscope guiding module, to position the laparoscope camera above the operation field Fig. 2.

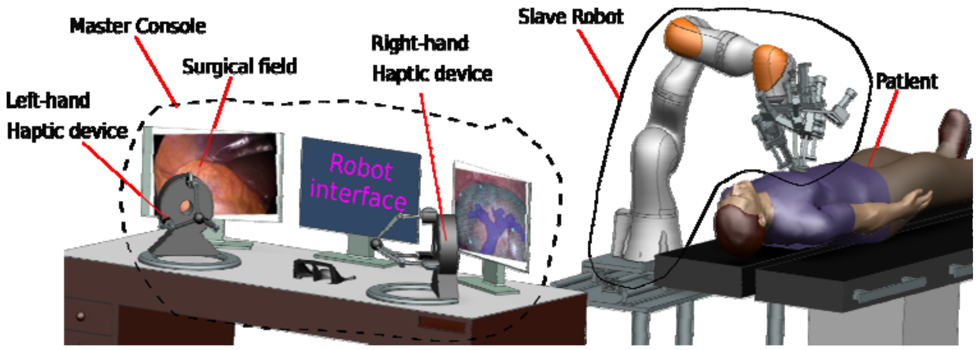

Fig. 1 – Master-slave robotic architecture in SILS [19].

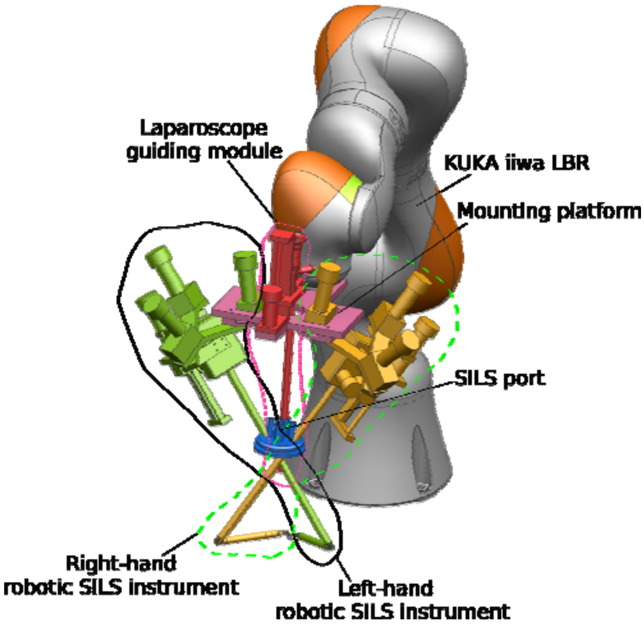

Fig. 2 – The SILS robotic system.

2.1. THE ROBOTIC INSTRUMENT FOR SILS

Fig. 3 illustrates a new concept design for a robotic assisted SILS instrument. It is based on a spherical mechanism, where the axis of rotation (in our case q_1 and q_2) intersect at the center of the mechanism (point O , where the coordinate system of the whole instrument is also placed). Point O represents the Remote Center of Motion (RCM) of the mechanism a concept that has been further described in [21–25], which is fixed and naturally maintains (due to the mechanism architecture), and which also serves as the insertion point into the SILS port, usually made of elastic polymers.

Besides the spherical mechanism, the instrument has an additional wrist with 3 DoF whose axes intersect in point P, namely: a rotation around PZ_3 axis (performed by the active joint q_3), a rotation around PX_4 axis (by q_4) and a rotation around the PZ_5 axis (by q_5). The active joint q_3 is directly actuated (using the motor M_3), while the joints q_4 and q_5 are cable actuated, using the motors M_4 and M_5 respectively, through a system of pulleys for cable guiding as in Fig. 4 Point P can translate along the OZ_3 axis, motion performed by the prismatic joint q_6.

The other geometric parameters of the robotic SILS instrument are: the angles δ_1 and δ_2 between the elements A_O (the instrument frame, which is fixed) and A_1, respectively A_1 and A_2, which are chosen so that the axis OZ_1, OZ_2 and OZ_3 intersect in the origin, point O; the length r, which represents the difference between the points O and P when $q_6 = 0$; the length b, between points P and E (the end-effector characteristic point).

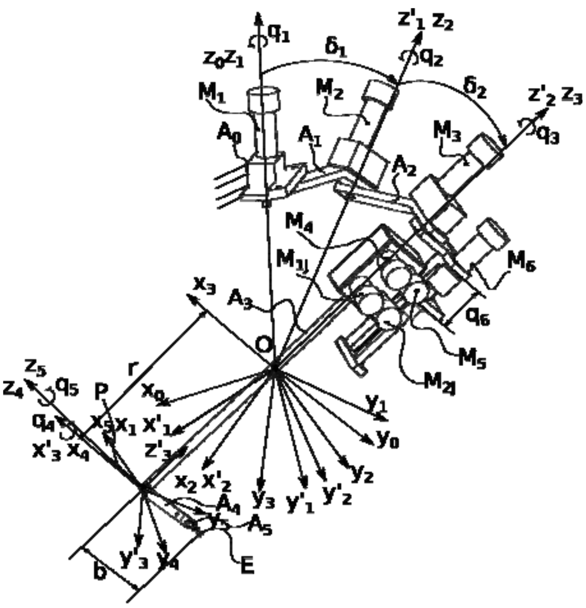

Fig. 3 – Kinematic scheme of SILS robotic instrument.

The instrument has $N = 5$ mobile elements (elements in motion), namely the elements A_1 to A_5 (element A_0 is the instrument frame, hence its position is fixed) the mechanism family (the number of common restrictions for all mobile elements of the mechanism) is $F = 3$ and that it has 4 class 5 (C_5) joints and one class 4 (C_4) – element A_3 can both rotate and translate along the OZ_3 axis, where 4 and 5 are the number of restricted motions for each joint, so using Eq. (1) the number of independent motions of the instrument (M) are computed as follows [26]:

$$M = (6 - F) \cdot N - \sum_{i=1}^{5} (i - F) \cdot C_i, \tag{1}$$

yielding:

$$M = 6, \tag{2}$$

therefore the instrument is capable to perform 6 independent motions.

Fig. 4 presents the system of pulleys used to guide the driving cables that perform the q_4 and q_5 rotations. It is important to mention that each jaw of the end-effector (a grasping one in this case) is actuated separately, using the motors M_{1J} and M_{2J}, Fig. 3, due to surgical procedure constrains.

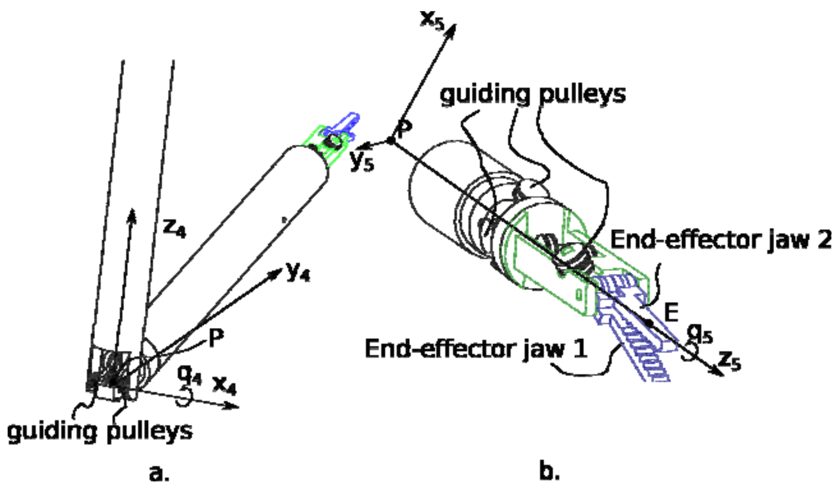

Fig. 4 – Robotic SILS instrument wrist and end-effector.

2.2. KINEMATIC ANALYSIS OF THE SILS INSTRUMENT

The kinematic parameters of the instrument are presented in Table 1 using a the Denavit-Hartenberg (D-H) notation, where q_i are the active joints [28]. When all q_i are set to 0 $(q_i = 0, i = 1...6)$, the spherical mechanism of the instrument is fully extended, meaning that when $q_1 = 0$ and $q_2 = 0$, Euler angles of rotation

$(Zx'z^*)$ $\psi = 0, \theta = \delta_1 + \delta_2$. Angle φ will be determined, as presented in the inverse kinematics subsection.

1. Forward kinematics. Starting from the mechanism parameters presented in Table 1, the forward kinematics leads to the pose of the end-effector (position and orientation) in the base coordinate system, placed in point *O* (also the RCM). This is easily obtained using Eq. (3), where ${}^{i-1}T_i$ represents the transformation matrix from the previous frame to the current one. The angle δ_0 between the axis OZ_0 and OZ_1 is zero (it is not symbolized in Fig. 3).

Table 1

SILS robotic instrument D-H parameters

Joint i	δ_{i-1}	d_{i-1}	q_i	r_i
1	δ_0	0	q_1	0
2	δ_1	0	q_2	0
3	δ_2	0	q_3	0
4	$\pi/2$	0	q_4	0
5	$\pi/2$	0	q_5	0
6	0	b	0	q_6+r

$$ {}^0T_6 = {}^0T_1 \cdot {}^1T_2 \cdot {}^2T_3 \cdot {}^3T_4 \cdot {}^4T_5 \cdot {}^5T_6 . \quad (3)$$

2. *Inverse kinematics*. Starting from coordinates of the end-effector and its orientation, expressed in the Euler angles (ψ,θ,φ), using the inverse kinematic model, the target is to determine the active joints displacements $(q_1...q_6)$. It is obvious that at least the spherical mechanism of the instrument will have multiple solutions, without even considering the redundancies (the active joints q_3 and q_5, both representing rotations around OZ_3 and OZ_5 axis). Nevertheless, an analytical solution may be obtained by splitting the instrument in two mechanisms: the spherical mechanism (including the q_1, q_2 and q_6 active joints) and the wrist consisting of the three active joints whose axis intersect in point P: q_3, q_4 and q_5. In addition, considering that the instrument will be controlled using the Omega.7 haptic device, this strategy of solving the inverse kinematics is even more natural: using the Delta mechanism of the haptic, one can control the orientation of the element A_3 (the spherical mechanism) and the position of point P, constrained by the RCM; using the Roll-Pitch-Yaw wrist of the haptic device, the wrist orientation of the instrument can be also controlled (q_3, q_4, q_5), leading to the final pose of the end-effector (point E) – Fig. 5.

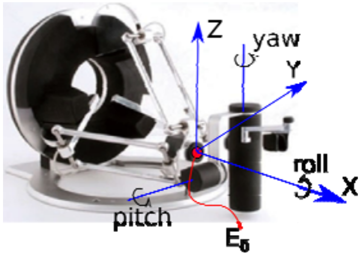

Fig. 5 – The Omega.7 haptic device for the control of the SILS robotic instrument.

The Euler angles ψ_1 and θ_1, defining the orientation of the A_3 element, can be obtained by imposing the position of point P and of the RCM (point O), as in Fig. 6. Using Eq. (4), a system of equations as in (5) can be obtained, which leads to the expressions of q_1, q_2, q_6 and the angle φ_1, considering that $\theta_1 > 0, \delta_1 > 0$ and $\delta_2 > 0$, and $S\beta = \sin(\beta)$, and $C\beta = \cos(\beta)$.

$$T(\psi_1)\cdot T(\theta_1)\cdot T(\varphi_1)\cdot T(P) = {}^0T_1 \cdot {}^1T_2 \cdot {}^5T_6, \tag{4}$$

$$\begin{cases} S\theta_1 C\varphi_1 - S\delta_1 Cq_2 C\delta_2 - C\delta_1 S\delta_2 = 0, \\ S\theta_1 C\psi_1 - \left(S\delta_2 Cq_2 C\delta_1 + C\delta_2 S\delta_1\right) Cq_1 - Sq_1 Sq_2 S\delta_2 = 0, \\ C\theta_1 + S\delta_1 Cq_2 S\delta_2 - C\delta_1 C\delta_2 = 0, \\ S\theta_1 S\varphi_1 X_P + S\theta_1 C\varphi_1 Y_P + C\theta_1 Z_P + \left(q_4 + r\right)\left(S\delta_1 Cq_2 S\delta_2 - C\delta_1 C\delta_2\right) = 0. \end{cases} \tag{5}$$

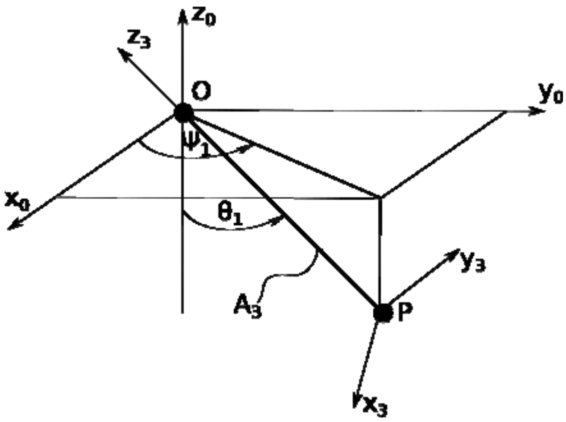

Fig. 6 – Determining the orientation of the element A_3.

Two solutions are obtained for each angle, as in Eq. (6), (7) and (8), the expression for q_1 being too large to be presented in this paper. Fig. 7 illustrates the two solutions of the spherical mechanism, for q_1 and q_2. Switching between the two possible configurations of the spherical mechanism is achievable by imposing additional constraints, such as $q_1 < \pi / 2$ and $q_2 > 0$.

$$\varphi_1 = \text{atan2}\left(\pm\sqrt{R_1}, C\delta_1 - C\delta_2 C\theta_1\right), \tag{6}$$

$$q_2 = \text{atan2}\left(\pm\sqrt{2C\delta_2 C\delta_1 C\theta_1 + \left(S\theta_1\right)^2 + \left(S\delta_1\right)^2 + \left(S\delta_2\right)^2}, C\delta_1 C\delta_2 + C\theta_1\right), \tag{7}$$

$$q_6 = \frac{-\left(C\theta_1\right)^2\left(Y_P C\delta_2 - Z_P S\delta_2 + rS\delta_2\right) + C\theta_1\left(Y_P C\delta_1 - X_P\sqrt{R_1}\right)}{\left(C\theta_1\right)^2 S\delta_2}, \tag{8}$$

where

$$R_1 = 2C\delta_2 C\delta_1 C\theta_1 + \left(S\theta_1\right)^2 - \left(C\delta_1\right)^2 - \left(C\delta_2\right)^2. \tag{9}$$

The q_3, q_4 and q_5 active joints expressions are obtained using (10). It is important to consider that the instrument has already performed a rotation around the OZ_3 axis with the φ_1 angle.

$$T\left(\psi_2\right)\cdot T\left(\theta_2\right)\cdot T\left(\varphi_2\right)\cdot T\left(E\right) = T\left(\varphi_1\right)\cdot {}^2T_3 \cdot {}^3T_4 \cdot {}^4T_5 . \tag{10}$$

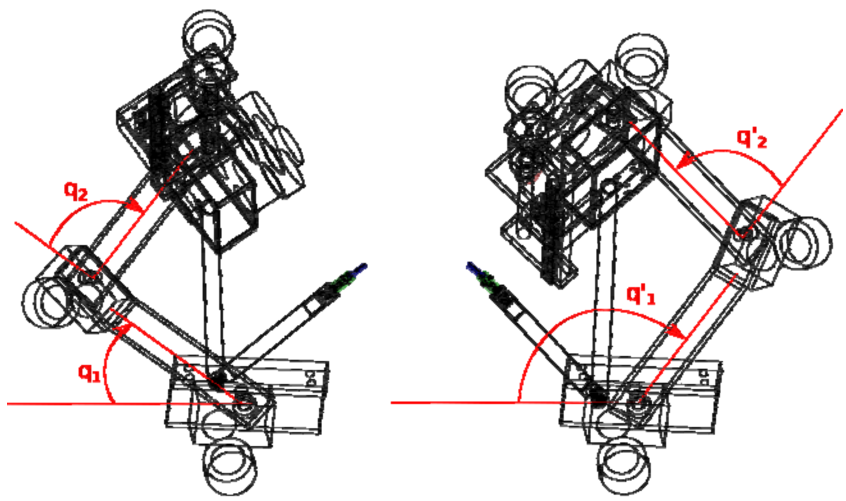

Fig. 7 – The two configurations corresponding to the two obtained solutions for q_1 and q_2.

This leads to the following solutions, accounting that the gimbal lock is avoided by imposing $\theta_2 < 0$ and $\varphi_2 < 0$:

$$q_3 = \text{atan2}\left(\pm - S\theta_2 C\varphi_2 S\varphi_1 + C\varphi_1 S\varphi_2, \pm S\theta_2 C\varphi_2 C\varphi_1 + S\varphi_1 S\varphi_2\right), \tag{11}$$

$$q_4 = \text{atan2}\left(\pm\sqrt{1-\left(C\theta_2\right)^2\left(C\varphi_2\right)^2}, \pm\sqrt{\left(C\theta_2\right)^2\left(C\varphi_2\right)^2}\right), \tag{12}$$

$$q_5 = \text{atan2}\left(\pm\sqrt{1-\left(C\theta_2 S\varphi_2 S\psi_2 + S\theta_2 C\psi_2\right)^2}, \pm C\theta_2 S\varphi_2 S\psi_2 + S\theta_2 C\psi_2\right). \tag{13}$$

3. THE CLIENT-SERVER COMMUNICATION ARCHITECTURE

The implementation of the master-slave teleoperation system assumes the development of an efficient communication architecture for a real-time operation of the slave robotic system. The work within this section is focused only on the control of the KUKA iiwa, but it can easily be extended for the control of the whole slave robotic system. Fig. 8 presents the main pillars of the developed communication architecture between the Omega.7 and the KUKA iiwa. On the server side the CHAI3D [29], which is one of the most important frameworks for the control of the haptic devices has been used, integrating the specific libraries for the Omega.7. On the client side the inverse kinematics model of the KUKA iiwa implemented within a MATLAB [30] script has been integrated into the architecture so that the creation of MEX-Files is avoided. Another MATLAB script is used to communicate with the CoppeliaSim [31], as an important tool used for the simulation of robot trajectories in a virtual environment.

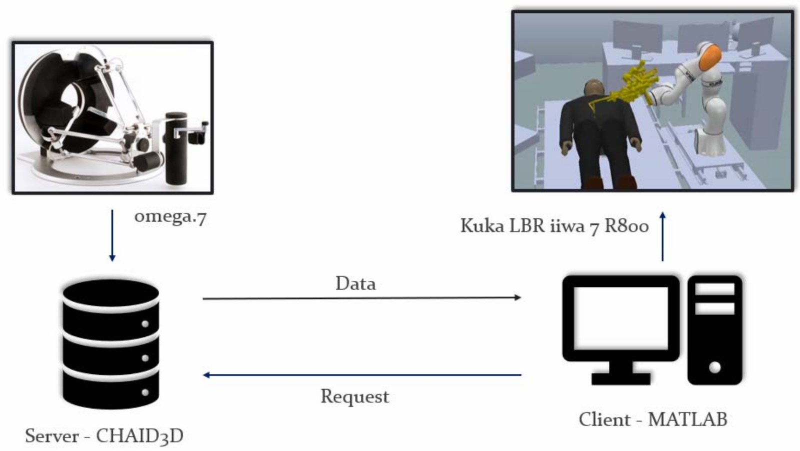

Fig. 8 – Communication Architecture.

The CHAI3D Module has been implemented in C++ and it consists of two threads:

- ✓ The main thread is used to get the data from the Omega.7 in terms of position and orientation. It sends data to the client (MATLAB script) using socket communication,
- ✓ The second thread is used to control the device itself.

Table 2 presents the structure of a communication package, specifying the fields of the packages specific for each byte. The first 3 bytes are used for the position in Euclidean coordinates (the E_δ coordinates in Fig. 5), while the next 9 bytes encapsulate the elements of the Rotation matrix that relate the base reference system to the wrist. The last byte is used to collect data regarding the grip angle of the Omega.7, which within this communication protocol, for the control of the KUKA iiwa has been implemented as a user button, its function being detailed in the next section.

The MATLAB module collects the data from the first thread of the server, unpacks it and using the KUKA iiwa inverse kinematics, the solution regarding the joint values for the robot is sent to CoppeliaSim using the remoteApi to simulate the robot motion for the generated trajectory.

Table 2

Packet's structure

Bytes	***Data types***
1-9	*position on x*
12-20	*position on y*
23-31	*position on z*
34-42	r_{11}
45-53	r_{21}
56-64	r_{31}
67-75	r_{12}
78-86	r_{22}
89-97	r_{32}
100-108	r_{13}
111-119	r_{23}
122-130	r_{33}
133-141	*gripper angle*

An overview of the MATLAB Module is illustrated in Fig. 9. The first two steps consist in the connection with the server (CHAI3D) and with the simulation environment (CoppeliaSim). After establishing a secured connection, the first thread within the CHAI3D Module constantly updates the Omega.7 data (regarding the position and orientation) and sends the packages to the MATLAB Module using the socket communication. The data is unpacked and using the KUKA iiwa inverse kinematics, the joint angles are computed and provided that the solution is feasible, these are sent to the Kuka iiwa using the CoppeliaSim's remoteApi in real-time.

An important issue that needs to be addressed during the KUKA iiwa operation with the Omega.7 consists in the large disproportion between the master and slave workspaces. Fig. 10 shows the workspace of the Omega.7 which has been measured on experimental basis, collecting a point cloud with the end-effector position during a motion on its boundary workspace. Obviously, the KUKA iiwa has a much larger workspace than the Omega.7, which required the implementation of the algorithm presented in Fig. 11, which has been developed so that the user can navigate with the Omega.7 in the Kuka iiwa's workspace.

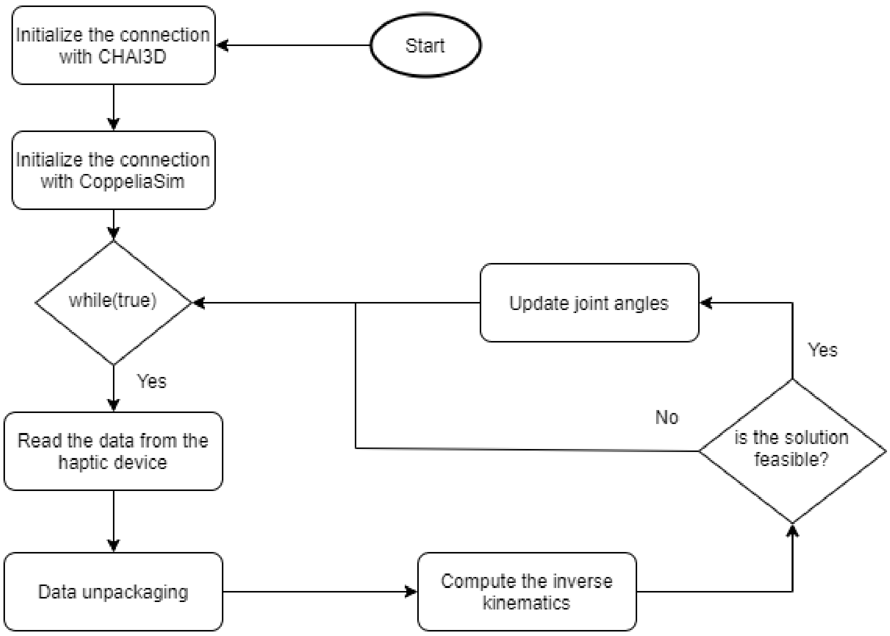

Fig. 9 – MATLAB Model overview.

When the simulation starts, the Kuka iiwa starting position has been settled to [0,0,0.95] while the Omega.7's origin to [0,0,0]. If the gripper angle (as a push button) has a value larger than zero (when the gripper is fully closed) the push button is considered not pressed and the KUKA iiwa's position will be determined using the equation showed in Fig. 11. If the push button is pressed the KUKA iiwa's starting position becomes the last known position of the robot and the origin of the Omega.7 frame becomes the last value read from the haptic device. It is mandatory to translate the base frame reference system of the Omega.7 to guarantee a continuous movement. Notice that when the button (Omega.7 gripper) has been pressed, the Kuka iiwa's position is not updated while moving the haptic device (the robot is still).

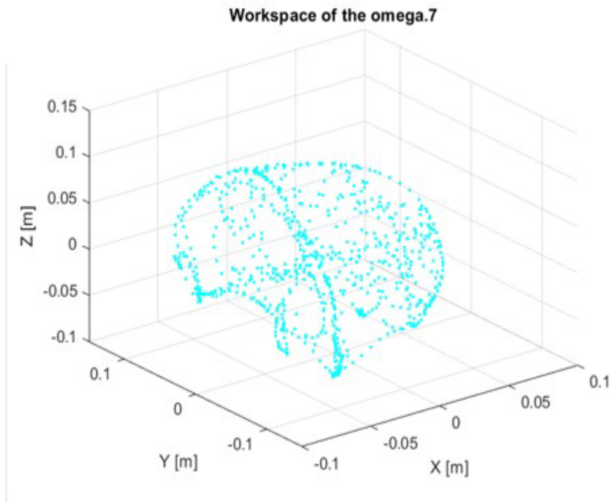

Fig. 10 – Omega.7 workspace experimentally determined.

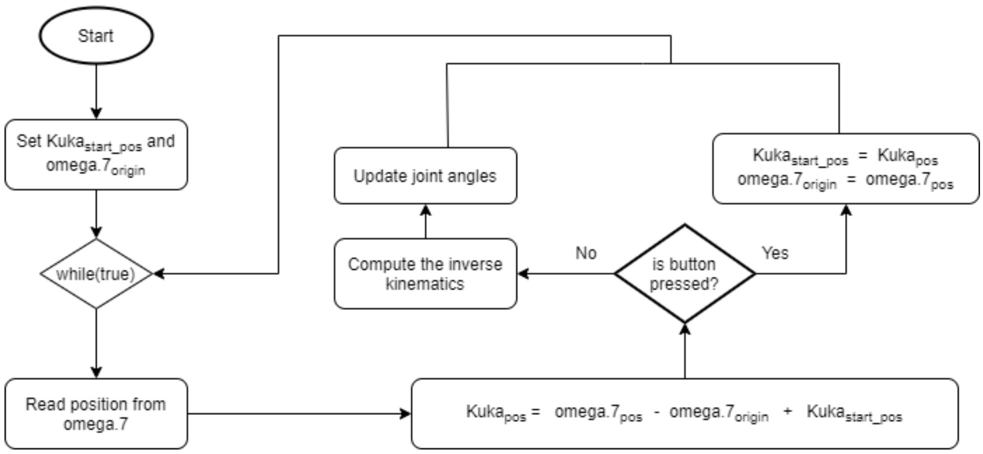

Fig. 11 – KUKA iiwa – Omega.7 workspace adaptation.

4. SIMULATIONS RESULTS

To illustrate how the MATLAB model described before, works, four simulations are presented:

- *Movement over x axis:* in which the Robot's trajectory imposed by the user is on the x-axis.
- *Movement over y axis:* in which the Robot's trajectory imposed by the user is on the y-axis.
- *Movement over y-axis with repositioning:* in which instead of the previous simulation the user navigates out of the omega.7 workspace using the adaption algorithm.
- *Real case simulation:* in which the user navigates with the Robot in the real environment to position the Robot over the patient.

For each simulation, the starting point has been settled to: [0, 0, 0.95] (m).

4.1. MOVEMENT ALONG *x* AND *y* AXIS

In the first simulation, as can be seen in the Fig. 12a. the user moves the Omega.7 haptic device on the x axis within the $x-y$ plane and Fig. 12b presents the trajectory of the Kuka iiwa, copying the motion of the Omega.7. In this case, the user button (the Omega.7 gripper) is never pressed by the user so that the starting position does not change and the base frame of the Omega.7 is not moved.

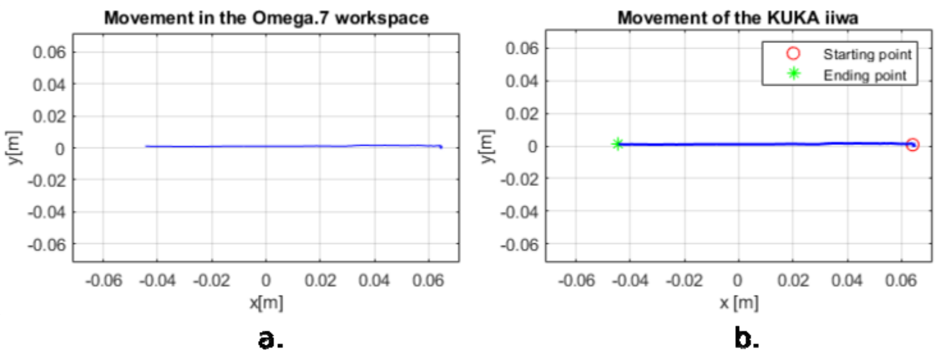

Fig. 12 – Motion trajectory on the x axis of the Omega.7 (a.) and the resulting motion of the KUKA iiwa end-effector (b.).

Fig. 13 and Fig. 14 presents the time history diagram of the Omega.7 Delta mechanism joints for the trajectory presented in Fig. 12a. and the resulting active joints variation of the Kuka iiwa.

In the second simulation, as can be seen in Fig. 13 the user moves the Omega.7 along the y-axis, while the KUKA iiwa copies the motion. In the $x-y$ plane, the movement of the Kuka iiwa and the movement of the Omega.7 are the same, because the starting position in the plane $x-y$ is [0,0] and because the user button is never pressed by the user. In Fig. 15a and Fig. 15b are showed the Omega.7 and the Kuka iiwa joint angles time history diagram, respectively.

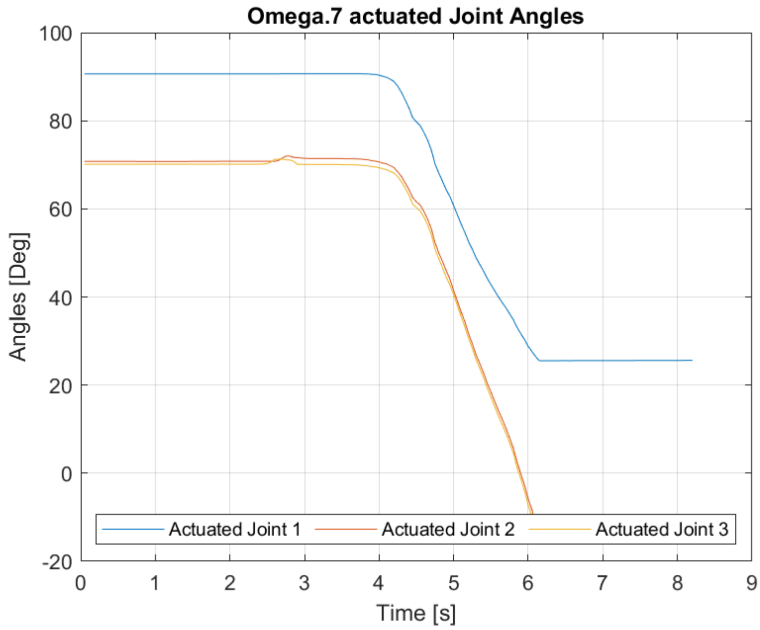

Fig. 13 – The Omega.7 Delta mechanism joints time history diagram.

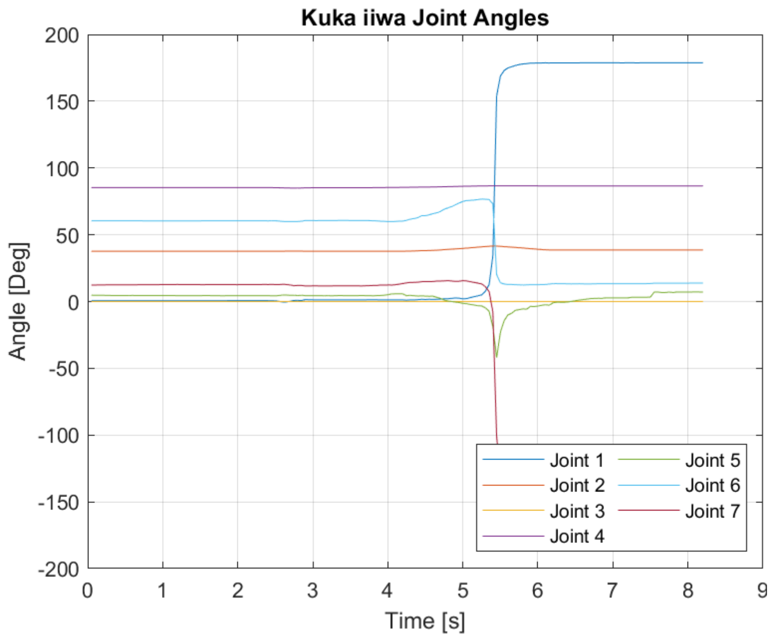

Fig. 14 – The KUKA iiwa joint angles time history diagram for the x axis motion of the Omega.7.

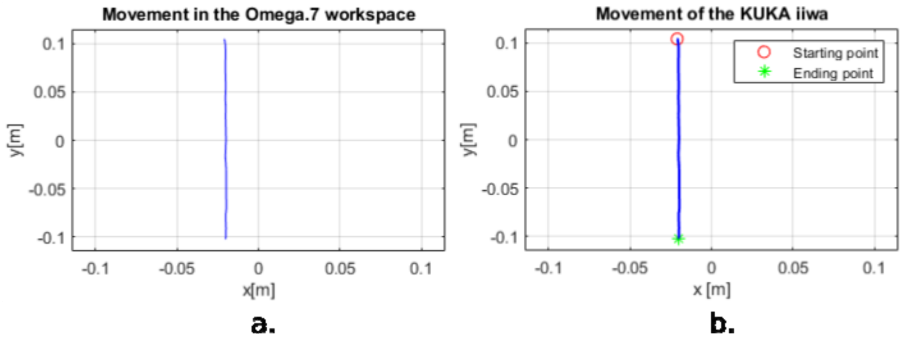

Fig. 15 – Motion trajectory on the x axis of the Omega.7 (a.) and the resulting motion of the KUKA iiwa (b.).

4.3 MOVEMENT OVER *y* AXIS WITH REPOSITIONING

The aim of the third simulation is to show how the workspace adaptation algorithm (Fig. 11) works. The task is to move the Omega.7 over the y-axis just as in the last simulation, but this time navigating over the KUKA iiwa workspace when the end-effector reaches the haptic device's workspace boundary.

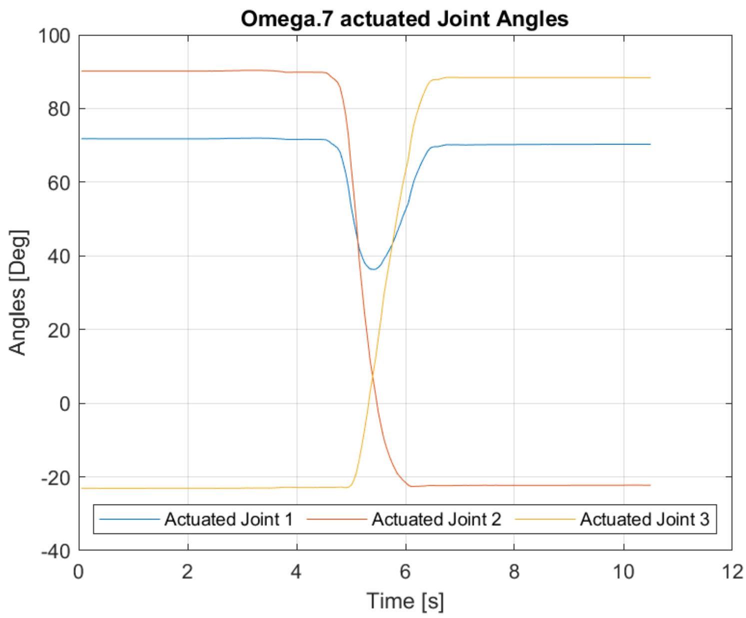

Fig. 16 – The Omega.7 Delta mechanism joints time history diagram for the *y*-axis motion.

As presented in Fig. 18, when the user reaches the Omega.7 workspace upper limit, the push button is being clicked and the Omega.7 is repositioned. During the repositioning, the Kuka iiwa is maintained still. In this simulation, the repositioning has been done two times, as it can be noticed the distance covered by the robot over the y-axis is three times the one covered by the Omega.7, Fig. 19.

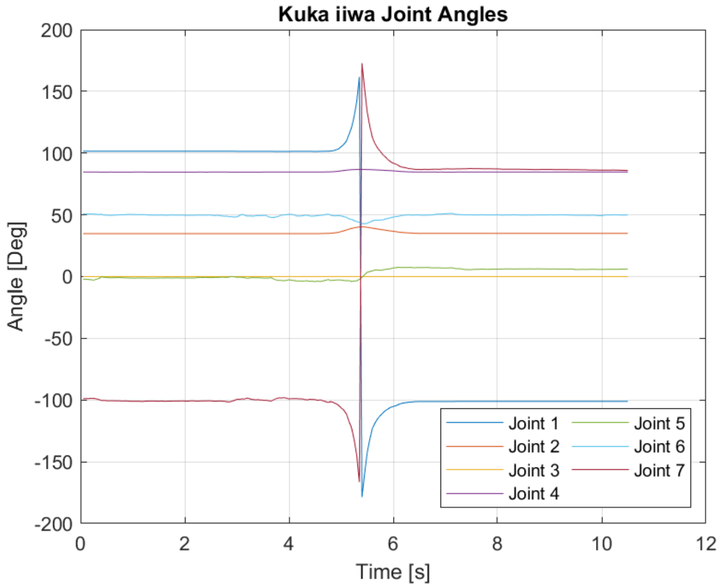

Fig. 17 – The KUKA iiwa joint angles time history diagram for the y-axis motion of the Omega.7.

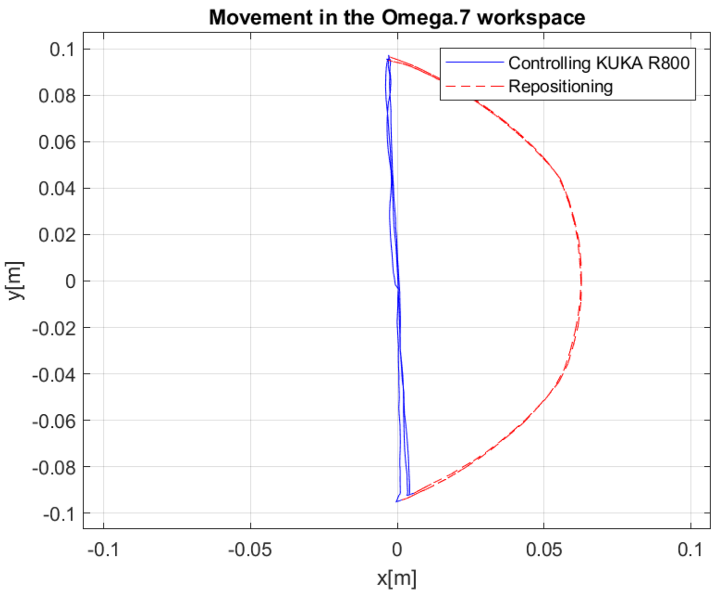

Fig. 18 - Moving the Omega.7 with repositioning (gripper button clicked).

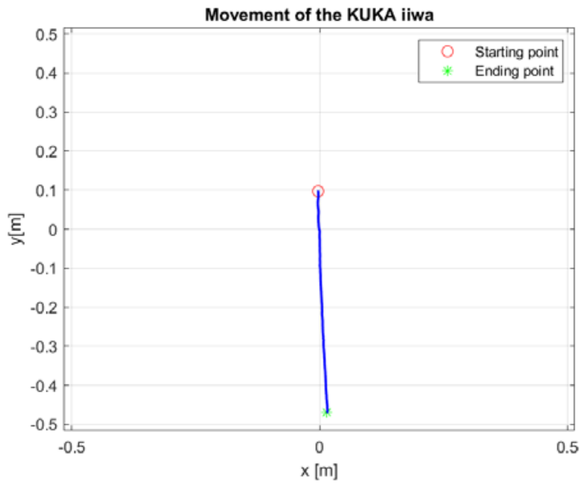

Fig. 19 – KUKA iiwa copying the motion of the Omega.7 with repositioning over *y*-axis.

4.4. REAL CASE SCENARIO SIMULATION

In this scenario the user's task is to position the KUKA iiwa with the robotic SILS instruments attached to it, within the medical environment, preparing for a urologic intervention. Four frames from CoppeliaSim have been showed in Fig. 20, in which:

- ✓ In frame 1 the Kuka iiwa is shown in the starting position,
- ✓ In frames 2 and 3 the Kuka iiwa is repositioned using the Omega.7 over the patient, preparing for the surgical intervention,
- ✓ In frame 4 the robot is preparing to position the SILS instruments at the surgical site (the SILS port is placed on the patient and the instruments will be inserted into the patient's body).

Fig. 21 presents the trajectory of the KUKA iiwa in the 3D space during the SILS instruments positioning simulation.

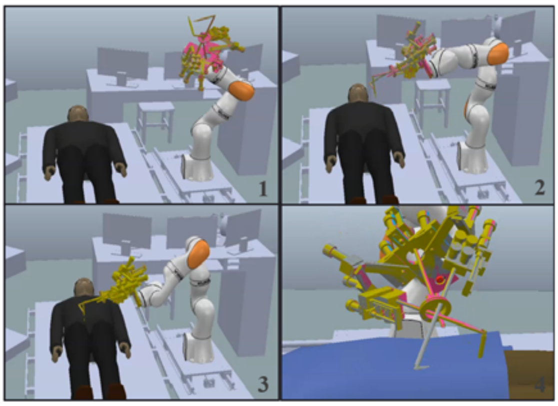

Fig. 20 – Moving the KUKA iiwa in the simulated medical environment.

5. CONCLUSION

The paper presents a robotic system designed for SILS interventions, using the master-slave teleoperation architecture. This work is usable in telemedicine to reduce the burden of adversities in efficient communication between medical professionals and patients, eventually providing faster and more cost-effective treatments. The robotic system consists of the KUKA iiwa collaborative robot used to position a set of dedicated robotic SILS instruments at the operation sites. The robotic SILS instrument has been designed and its forward and inverse kinematics presented in a way that fits the implementation of a control system using the Omega.7 haptic device. Furthermore, a novel client-server communication architecture to interface the Omega.7 with the other environments, namely MATLAB, and CoppeliaSim has been developed. The use of the socket communication is useful to avoid software integration problems and a viable solution has been implemented to map the two main components workspaces (the KUKA iiwa and the Omega.7) with minimum risk and maximum convenience for the user. The main advantage of the presented telemedicine research prototype is that it can integrate a haptic device with a VR environment that can easily be translated into a real-case scenario once all the components of the robotic system are developed.

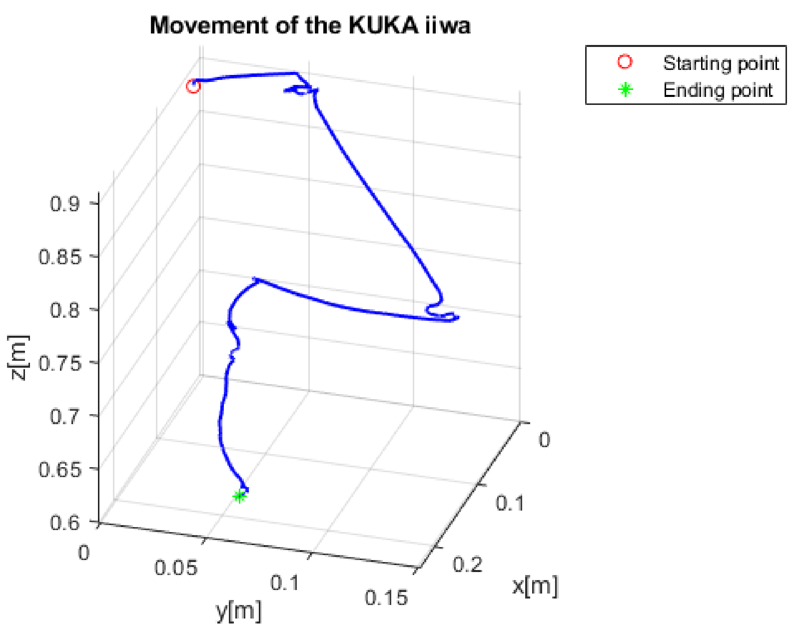

Fig. 21 – The KUKA iiwa trajectory during SILS instruments positioning.

Acknowledgements. This work was supported by a grant of the Ministry of Research, Innovation and Digitization, CNCS/CCCDI – UEFISCDI, project number PCE171/2021 – Challenge within PNCDI III.

Received on 28 July, 2021

REFERENCES

1. SUZUKI, Y., WAKASUGI, M., MIKAMORI, M., TAMAOKA, K., NAKAHARA, Y., TEI, M., FURUKAWA, K., OHTSUKA, M., MASUZAWA, T., AKAMATSU, H., *Long-term outcomes of single-incision versus multiport laparoscopic totally extra-peritoneal inguinal hernia repair: a single-institution experience of 186 consecutive cases*, Surg Today, 2021 Jun 11, doi: 10.1007/s00595-021-02323-4. Epub ahead of print. PMID: 34115209.
2. CHEM, B.S.M., LAKHOTIA, S., KHOO, C.K., SIOW, A.Y.M., *Single incision laparoscopic surgery in gynecology: Evolution, current trends, and future perspectives*, Gynecol. Minim. Invasive Ther., **1**, pp. 9–18, 2012.
3. PETRONI, G., NICCOLINI, M., MENCIASSI, A., DARIO, P., CUSCHIERI, A., *A novel intracorporeal assembling robotic system for single-port laparoscopic surgery*, Surg. Endosc., **27**, *2*, pp. 665–670, 2013.
4. WORTMAN, T.D., MONDRY, J.M., FARRITOR, S.M., OLEYNIKOV, D., *Single-site colectomy with miniature in vivo robotic platform*, IEEE Trans Biomed. Eng., **60**, *4*, pp. 926–929, 2013.
5. YUNG, K.L., CHEUNG, J.L.K., CHUNG, S.W., SINGH, S, YEUNG, C.K., *A singleport robotic platform for laparoscopic surgery with a large central channel for additional instrument*, Ann. Biomed. Eng., **45**, *9*, pp. 2211–2221, 2017.
6. KOBAYASHI, Y., SEKIGUCHI, Y., NOGUCHI, T., TAKAHASHI, Y., LIU, Q., OGURI, S., TOYODA, K., UEMURA, M., IEIRI, S., TOMIKAWA, M., OHDAIRA, T., HASHIZUME, M., FUJIE, M.G., *Development of a robotic system with six-degrees-of-freedom robotic tool manipulators for single-port surgery*, Int. J. Med. Robot, **11**, *2*, pp. 235–246, 2015.
7. CHEON, B., GEZGIN, E., JI, D.K., TOMIKAWA, M., HASHIZUME, M., KIM, H.J., HONG, J., *A single port laparoscopic surgery robot with high force transmission and a large workspace*, Surg. Endosc., **28**, *9*, pp. 2719–2729, 2014.
8. XU, K., GOLDMAN, R.E., DING, J., ALLEN, P.K., FOWLER, D.L., SIMAAN, N., *System design of an insertable robotic effector platform for single port access (SPA) surgery*. IEEE/RSJ International Conference on Intelligent Robots and Systems (IROS), pp. 5546–5552, 2009.
9. XU, K., ZHAO, J., FU, M., *Development of the SJTU unfoldable robotic system (SURS) for single port laparoscopy*, IEEE/ASME Trans. Mechatron, **20**, *5*, pp. 2133–2145, 2015.
10. DOBBS, R.W., HALGRIMSON, W.R., TALAMINI, S., VINGESWARAN, H.T., WILSON, J.O., CRIVELLARO, S., *Single-port robotic surgery: the next generation of minimally invasive urology*, World J. Urol. Apr., **38**, *4*, pp. 897–905, 2020, doi: 10.1007/s00345-019-02898-1. Epub 2019 Aug 28. PMID: 31463560.
11. ELLI, E., GONZALES-HEREDIA, R., SARVEPALLI, S., MASRUR, M., *Laparoscopic and robotic sleeve gastrectomy: short- and long-term results*, Obes Surg., **25**, *6*, pp. 967–974, 2015, doi: 10.1007/s11695-014-1499-0. PMID: 25417069.
12. HAGEN, M.E., BALAPHAS, A., PODETTA, M., ROHNER, P., JUNG, M.K., BUCHS, N.C., BUEHLER, L., MENDOZA, J.M., MOREL, P., *Robotic single-site versus multiport laparoscopic cholecystectomy: a case-matched analysis of short- and long-term costs*, Surg. Endosc., **32**, *3*, pp. 1550–1555, 2018, doi: 10.1007/s00464-017-5843-z. Epub 2017 Oct 19. PMID: 29052069.

13. LEVIC, K, DONATSKY, A.M., BULUT, O., ROSENBERG, J., *A Comparative Study of Single-Port Laparoscopic Surgery Versus Robotic-Assisted Laparoscopic Surgery for Rectal Cancer*, Surg. Innov. Aug., **22**, *4*, pp. 368–375, 2015, doi: 10.1177/1553350614556367. Epub 2014 Nov 5. PMID: 25377216.
14. LOPEZ, S, MULLA, Z.D., HERNANDEZ, L., GARZA, D.M., PAYNE, T.N., FARNAM, R.W., *A Comparison of Outcomes Between Robotic-Assisted, Single-Site Laparoscopy Versus Laparoendoscopic Single Site for Benign Hysterectomy*, J. Minim Invasive Gynecol., **23**, *1*, pp. 84–88, 2016, doi: 10.1016/j.jmig.2015.08.883. Epub 2015 Aug 29. PMID: 26321172.
15. CORRADO, G., CUTILLO, G., MANCINI, E., BAIOCCO, E., PATRIZI, L., SALTARI, M., DI LUCA SIDOZZI, A., SPERDUTI, I., POMATI, G., VIZZA, E., *Robotic single site versus robotic multiport hysterectomy in early endometrial cancer: a case control study*, J. Gynecol. Oncol. Jul., **27**, *4*:e39., 2016, doi: 10.3802/jgo.2016.27.e39. PMID: 27171672; PMCID: PMC4864515.
16. VAIDA, C., PISLA, D., PLITEA, N., GHERMAN, B., GUYRKA, B., *Development of a Control System for a Parallel Robot used in Minimally Invasive Surgery*, IFMBE Proc., **26**, pp. 171–176, 2009, doi: 10.1007/978-3-642-04292-8_38.
17. GALDAU, B., PLITEA, N., VAIDA, C., COVACIU, F., PISLA, D., *Design and control system of a parallel robot for brachytherapy*, Proceedings of IEEE International Conference on Automation, Quality and Testing, Robotics. pp 1–6, 2014.
18. VAIDA, C., PISLA, D., COVACIU, F., GHERMAN, B., PISLA, A., PLITEA, N., *Development of a control system for a HEXA parallel robot*, IEEE International Conference on Automation, Quality and Testing, Robotics (AQTR), pp. 1–6, 2016, doi: 10.1109/AQTR.2016.7501318.
19. PISLA, D., ANDRAS, I., VAIDA, C., CRISAN, N., ULINICI, I., BIRLESCU, I., PLITEA, N., *New approach to hybrid robotic system application in single incision laparoscopic surgery*, ACTA TECHNICA NAPOCENSIS, Series: Applied Mathematics, Mechanics, and Engineering, Accepted for publication, 2021.
20. BAGHDADI, A., HOSHYARMANESH, H., DE LOTBINIERE-BASSETT, M., CHOI, S.K., LAMA, S., SUTHERLAND, G., *Data analytics interrogates robotic surgical performance using a microsurgery-specific haptic device*, Expert Review of Medical Devices., **17**, *7*, pp. 721–730, 2020.
21. PISLA, D., GHERMAN, B., PLITEA, N., GYURKA,B., VAIDA, C., VLAD, L., GRAUR, F., RADU, C., SUCIU, M., SZILAGHI, A., STOICA, A., *PARASURG hybrid parallel robot for minimally invasive surgery*, Chirurgia, **106**, *5*, pp. 619–625, 2011.
22. PISLA, D., PLITEA, N., GHERMAN, B., VAIDA, C., PISLA, A., SUCIU, M., *Kinematics and design of a 5-DOF parallel robot used in minimally invasive surgery*, Advances in Robot Kinematics: Motion in Man and Machine, pp. 99–106, 2010.
23. VAIDA, C., PISLA, D., PLITEA, N., GHERMAN, B., GYURKA, B., STANCEL, E., HESSELBACH, J., RAATZ, A., VLAD, L., GRAUR, F., *Development of a control system for a parallel robot used in minimally invasive surgery*, IFMBE Proceedings, **26**, pp. 171–176, 2009.
24. PISLA, D., PLITEA, N., GHERMAN, B., VAIDA, C., PISLA, A., SUCIU, M., *Kinematics and design of a 5-DOF parallel robot used in minimally invasive surgery*, Advances in robot kinematics: Motion in man and machine, pp. 99–106, 2010.
25. GHERMAN, B., VAIDA, C., PISLA, D., PLITEA, N., GYURKA, B., LESE, D., GLOGOVEANU, M., *Singularities and Workspace Analysis for a Parallel Robot for Minimally Invasive Surgery*, IEEE International Conference on Automation, Quality and Testing, Robotics (AQTR), pp. 1–6, 2010, doi: 10.1109/AQTR.2010.5520866.
26. VAIDA, C., PLITEA, N., GHERMAN, B., SZILAGHYI, A., GALDAU, B., COCOREAN, D., COVACIU, F., PISLA, D., *Structural Analysis and Synthesis of Parallel Robots for Brachytherapy*, New Trends in Medical and Service Robots. Mechanisms and Machine Science, **16**, pp. 191–204, 2014.

27. SCHONSTEIN, C., *Kinematic control functions for a serial robot structure based on the time derivative Jacobian matrix*, Acta Technica Napocensis, Series: Applied Mathematics and Mechanics, **61**, *II*, pp. 219–224, 2018.
28. SCHONSTEIN, C., PANC, N., *Establishing the Jacobian matrix for a three degrees of freedom serial structure*, Acta Technica Napocensis, Series: Applied Mathematics and Mechanics, **61**, *I*, pp. 93–98, 2018.
29. WEI, L., NAJDOVSKI, Z., ZHOU, H., DESHPANDE, S., NAHAVANDI, S., *Extending support to customised multi-point haptic devices in CHAI3D*, Conf. Proc. - IEEE Int. Conf. Syst. Man Cybern., January, pp. 1864–1867, 2014.
30. CORKE, P., *MATLAB toolboxes: robotics and vision for students and teachers*, in *IEEE Robotics & Automation Magazine*, **14**, *4*, pp. 16–17, Dec. 2007, doi: 10.1109/M-RA.2007.912004.
31. ROHMER, E., SINGH, S.P.N., FERRSE, M., *V-REP: A versatile and scalable robot simulation framework*, IEEE/RSJ International Conference on Intelligent Robots and Systems, pp. 1321–1326, 2013, doi: 10.1109/IROS.2013.6696520.